Heliyon 10 (2024) e28646

Contents lists available at ScienceDirect

Heliyon

journal homepage: www.cell.com/heliyon

Research article

Evolution of structural and electronic properties standardized description in rhenium disulfide at the bulk-monolayer transition

Aleksey Baglov [a,b], Liudmila Khoroshko [a,b,*], Anastasiya Zhoidzik [a], Mengge Dong [c,d], Qunhong Weng [e], Mohsin Kazi [f], Mayeen Uddin Khandaker [g,h], Mohammad Aminul Islam [i], Zaira Zaman Chowdhury [j], M.I. Sayyed [k], Sergei Trukhanov [l], Daria Tishkevich [l], Alex Trukhanov [l]

[a] Belarusian State University, Faculty of Physics, 4 Nezavisimosti Av., Minsk, 220030, Belarus
[b] Belarusian State University of Informatics and Radioelectronics, P. Browka 6, Minsk, 220013, Belarus
[c] Department of Resources and Environment, School of Metallurgy, Northeastern University, Liaoning Province, Shenyang, 110819, PR China
[d] Department of Civil and Environmental Engineering, The Hong Kong Polytechnic University, Hong Kong SAR
[e] College of Materials Science and Engineering, Hunan University, 2 Lushan S Rd, Changsha 410082, PR China
[f] Department of Pharmaceutics, College of Pharmacy, POBOX- 2457, King Saud University, Riyadh-11451, Saudi Arabia
[g] Applied Physics and Radiation Technologies Group, CCDCU, School of Engineering and Technology, Sunway University, Bandar Sunway 47500, Selangor, Malaysia
[h] Faculty of Graduate Studies, Daffodil International University, Daffodil Smart City, Birulia, Savar, Dhaka 1216, Bangladesh
[i] Department of Electrical Engineering, Faculty of Engineering, Universiti Malaya, Jalan Universiti, 50603 Kuala Lumpur, Malaysia
[j] Nanotechnology and Catalysis Research Center, Institute of Advanced Studies, University of Malaya, 50603 Kuala Lumpur, Malaysia
[k] Department of Physics, Faculty of Science, Isra University, 1162 Amman, Jordan
[l] SSPA "Scientific-Practical Materials Research Centre of NAS of Belarus", Minsk, 220072, Belarus

ARTICLE INFO

Keywords:
Rhenium disulfide
Slab
Monolayer
Density functional theory
Pseudopotential theory
electronic structure
Density of states
molecular orbitals
electronic density

ABSTRACT

The structural and electronic properties of ReS_2 different forms — three-dimensional bulk and two-dimensional monolayer — were studied within density functional theory and pseudopotentials. A method for standardizing the description of bulk unit cells and "artificial" slab unit cells for DFT research has been proposed. The preference of this method for studying zone dispersion has been shown. The influence of the vacuum layer thickness on specified special high-symmetry points is discussed. Electron band dispersion in both classical 3D Brillouin zones and transition to 2D Brillouin zones in the proposed two-dimensional approach using the Niggli form of the unit cell was compared. The proposed two-dimensional approach is preferable for low-symmetry layered crystals such as ReS_2. It was established that the bulk ReS_2 is a direct gap semiconductor (band gap of 1.20 eV), with the direct transition lying in the X point of the first Brillouin zone, and it is in good agreement with published experimental data. The reduction in material dimension from bulk to monolayer was conducted with an increasing band gap up to 1.45 eV, with a moving direct transition towards the Brillouin zone center. The monolayer of ReS_2 is a direct-gap semiconductor in a wide range of temperatures, excluding only a narrow range at low temperatures, where it comes as a quasi-direct gap semiconductor. The transition, situated directly in the Γ-point, lies 3.3 meV below the first direct transition located near this point. The electronic density of states of ReS_2 in the bulk and monolayer cases of ReS_2 were analyzed. The molecular orbitals were built for both types of ReS_2 structures as well as the electron difference

* Corresponding authorBelarusian State University, Faculty of Physics, Minsk, Belarus. .
E-mail address: l.s.khoroshko@gmail.com (L. Khoroshko).

https://doi.org/10.1016/j.heliyon.2024.e28646
Received 15 December 2023; Received in revised form 21 March 2024; Accepted 21 March 2024
Available online 26 March 2024

density maps. For all types of ReS_2 structures, an analysis of populations according to Mulliken and Voronoi was carried out. All calculated data is discussed in the context of weak quantum confinement in the 2D case.

1. Introduction

Transition metal dichalcogenides (TMDs) have long attracted the interest of a significant number of researchers due to their unique combination of layered structure and electronic properties, which make them promising for various applications.

Among TMDs, disulfides of molybdenum (MoS_2) and tungsten (WS_2) are the most investigated ones, which were studied as catalysts for hydrogen production by electrochemical decomposition of water [1,2], as part of composites for anodes of lithium-based batteries [3], as materials for creating gas sensors [4], and transistors of subnanometer "post-silicon" electronics [5], etc. In addition, cross-doped materials of the MoO_3–MoS_2 system as well as its layered heterosystems are investigated as perspective z-scheme catalysts [6–8].

At the same time, rhenium disulfide (ReS_2) has been studied to a much lesser extent, although the material could be characterized as very promising according to the published articles at the moment. In addition to the use of nanostructured rhenium disulfide as a promising (photo) catalyst [9,10], one can note the formation of vertically oriented ReS_2 nanosheet arrays by chemical vapor deposition, which is promising for the creation of lithium-sulfur batteries with a small capacity loss per charge/discharge cycle [11]. Also, this material in the ultrathin film form was used in the design of a highly sensitive detector of polarized light [12] and a phototransistor [13]. The possibility of using ReS_2 to make field-effect transistors [14] is equally intriguing. The most complete generalization of the experimentally and theoretically studied properties of rhenium disulfide and its possible practical applications is contained in reviews by Rahman et al. [15] and recently by Satheesh et al. [16]. And as far as the authors know, no new review articles on this material have been published in scientific journals at the moment.

Although rhenium, molybdenum, and tungsten disulfides are layered materials, there are significant differences in their structures: ReS_2 crystals belong to the triclinic crystal system [16], while MoS_2 and WS_2 crystals are hexagonal [17,18]. The distortion inherent in the low-symmetry ReS_2 unit cell makes it a promising material for creating the element base of straintronics. The possibility of replacing sulfur ions in ReS_2 with ions of other chalcogens suggests the potential of creating solid solutions of triple rhenium chalcogenides with varied physicochemical properties in a relatively wide range of values.

The electronic properties of ReS_2 and $ReSe_2$ have been studied earlier by both calculations and experiments. In the paper [19], ReS_2 and $ReSe_2$ with distorted 1T structure – 1T′ were studied. It was shown that these materials are indirect semiconductors, calculated electronic density of states is in good agreement with experimental data obtained by ultraviolet photoelectron spectroscopy, but the electronic bands dispersion was not calculated. In the paper [20], a monolayer $ReSe_2$ with 1T′-structure has been studied in both density functional theory (DFT) and angle-resolved photoelectron spectroscopy (ARPES) approaches. It was shown that Re-$5d_{z2}$-states and Se-$3p_z$-states do not contribute significantly to the top of the valence band along the K–Γ–M (M–Γ–M) dispersion directions. In the paper [21], the narrow-band anisotropic electronic structure of 1T–ReS_2 was studied in the DFT calculations and in the ARPES experiment. The authors reported that this material is a direct semiconductor, and Re-$5d_{3z2-r2}$–states contribute a significant weight near the valence band maximum. In the paper [22], bulk ReS_2 and $ReSe_2$ were studied by DFT calculations, and it was shown that this material is an indirect semiconductor with a complicated band structure and nature of inter- and intraband transitions. These results are consistent with our own calculations of the crystal structure and electronic properties of bulk ReS_2 except for the fact that in our study, ReS_2 is a direct semiconductor [23]. The problem with direct/indirect semiconductor types in DFT calculations is related to the opacity data used as input parameters for structure. The used input structures may look similar, but in terms of crystalline symmetry, they are not close. Even small differences between ionic positions can lead to a change in the electronic band dispersion and semiconductor type. In addition, in our work [20], among others, we proposed the hypothesis that this material can exist in a few modifications with a small difference in structure due to a "smooth" energetic landscape with a few local minima, which also leads to discrepancies in the analysis obtained the calculated results. Another source of discrepancy is the experimental data. Most authors refer to two works that describe the experimentally obtained structural properties of rhenium dichalcogenides [24,25]. The main discrepancy is related to the fact that in the first paper, the ReS_2 structure contains 6 unique ions [24], while in the second it contains 12 [25]. Thus, consistent and correct analysis of theoretical and experimental investigations in the case of rhenium dichalcogenides is always difficult. As a result, the electronic bands' dispersion is inconsistent with true due to high-symmetry points for the first Brillouin zone (BZ) for hexagonal and triclinic syngonies that do not match. Although such fundamental parameters as band gap width and type of first electronic transition can be generally reproduced [19–23].

At the same time, the role of rhenium and sulfur ions in the configuration of the electronic structure has not been systematically studied. Also, the influence of dimensionality reduction from bulk (three-dimensional) to one or a few monolayers (two-dimensional) on structural and electronic properties practically wasn't investigated.

Thus, this work aims at solving several problems. Firstly, it proposes a consistent and unified structural model of the ReS_2 crystal (and related compounds) for the three- and two-dimensional cases for subsequent numerical calculations. Then the proposed structural approach will be used to comprehensively and systematically study the electronic properties of bulk ReS_2 using ab initio methods. Lastly, to study the influence of the quantum confinement effect when reducing the dimension of the ReS_2 to the limiting case – a monolayer. Analyzing the results and comparing them to known data will also be conducted.

2. Structural model

Bulk rhenium disulfide has a pinacoidal (centrosymmetric) unit cell belonging to the triclinic syngony with the $P\bar{1}$ space group. According to the paper [24], the primitive cell contains six unique ions: two of rhenium and four of sulfur. The Wyckoff position is 2i for all ions, which gives a total of 12 ions and 4 formulae units. As is known [25], in the triclinic system, all cell vectors are unequal in length. In addition, all angles between cell vectors must be different and must not include 90°. This allows for replacement of some vectors with others and, thus, the description of the same crystal structure by several variants of lattice vectors and angles between them. More facts about standardization attempts can be found in Parthé's book [26].

An alternative approach to simple permutations of cell vectors and their angles is to use the reduced form of the unit cell – the so-called cell in Niggli form, or Niggli-reduced cell, or just Niggli cell. According to the Niggli form of the unit cell [24], we understand that the three-dimensional Bravais lattice unit cell is based on the reduction theory of the positive definite quadratic forms [28–30]. Note that the transformation of the unit cell to Niggli form saves cell volume, but cell vectors, their angles, and ionic positions can change. But the source unit cell and the Niggli-reduced cell are equivalent mathematically. The importance of the Niggli cell lies in its uniqueness and in the possibility of determining the Bravais type of lattice by its use [31,32]. However, as is known [27], it is not easy to obtain. In the paper [27], there is a detailed description of the reduction procedure, the algorithm, and an example transformation.

To carry out the transformation procedure from the original (source) ReS_2 unit cell to the Niggli-reduced cell, we utilized the STRUCTURE TIDY program, originally developed by Gelato and Parthé [33], which is provided as third-party software in binary form along with the VESTA (**V**isualization for **E**lectronic and **ST**ructural **A**nalysis) package [34]. The appearance of the original ReS_2 unit cell in the source form as published in Ref. [16] and in the reduced Niggli form is shown in Fig. 1 (a, b). The lattice parameters and ionic positions for both cases are given in Tables 1 and 2.

As we can see, the transformation from a source unit cell to a reduced unit cell is accompanied by a change in the ReS_2 layer propagation plane. Originally, layer propagation direction was perpendicular to axis a. After transformation, it was perpendicular to axis b. Wyckoff positions were transformed either by permutation only (x ↔ y coordinates) or by permutation and modification (z coordinates). Only one cell vector was permutated and transformed (b ↔ a), while vector a is only permuted to b without transformation, and vector c is not changed. According to the cell vectors, the permutation angles were rearranged with a small change in their values. We will use a unit cell of bulk ReS_2 in the reduced Niggli form described above for our subsequent investigation of first-principles calculations.

The transition from a three-dimensional shape (bulk) to a two-dimensional shape in layered TMDs is often described in terms of decreasing the number of layers to a few or even one as a limit case.

Since many solid-state codes work only with three-dimensional periodic boundary conditions, modeling true two-dimensional systems with them is a difficult problem. Fortunately, there is a method that allows the study of these systems without significant cost that is ubiquitously used to describe ultrathin films, 1D structures, and surfaces – the slab model approach [35–37]. In the case of layered materials, we manually add a vacuum layer, typically 12–15 Å, in a direction perpendicular to the layer propagation. This vacuum layer turns off interactions between replicas of a unit cell in a modified direction (more precisely, it tends to zero). This is easy to do in the case of hexagonal materials (MoS_2, WSe_2, etc.), but not in the case of low-symmetric crystals such as ReS_2. Adding a vacuum layer changes the length of one of the cell vectors by a few times while saving the remaining vectors and the angles between them. However, this new "artificial" unit cell no longer satisfies Niggli form conditions, which was true for bulk material. Therefore, for a slab unit cell, it is necessary to repeat the reducing process, which can greatly change its shape.

In order to evaluate the quantum confinement effect in ReS_2, we studied the structural and electronic properties of ReS_2 in a two-dimensional case. We are considering the limited form of a two-dimensional case – a monolayer – a promising and important form of

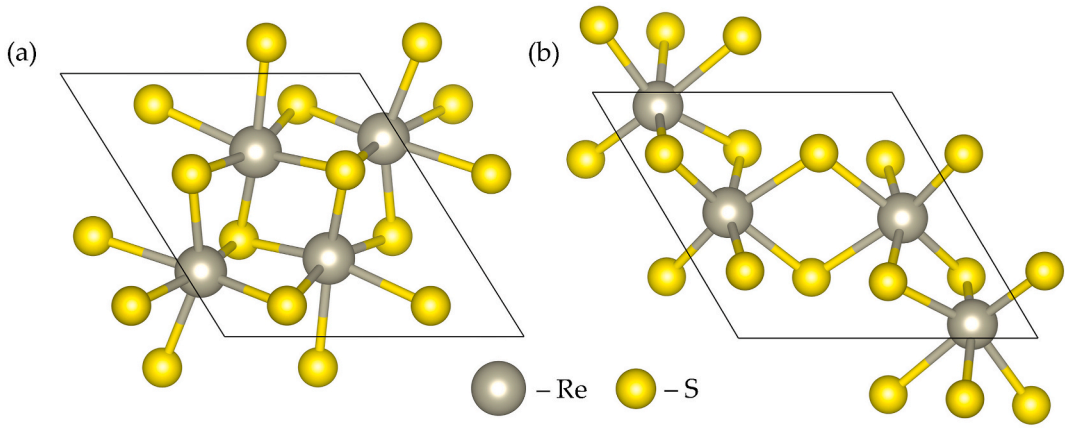

Fig. 1. Appearance of an original unit cell of bulk ReS_2 in (100) direction (a). Appearance in (010) direction after reducing the original unit cell to Niggli form (b). The original unit cell was created from experimental data presented in the paper [21]. The selected view is perpendicular to the direction of layer propagation.

Table 1
Wyckoff position of rhenium and sulfur ions for original and Niggli-reduced cells.

Unique atom	Wyckoff positions					
	Published data			Reduced form		
	x	y	z	x	y	z
Re1	0.4925	0.0564	0.2477	0.0564	0.4925	0.8087
Re2	0.5026	0.5112	0.2974	0.5112	0.5026	0.2138
S1	0.2174	0.2498	0.3676	0.2498	0.2174	0.8822
S2	0.2769	0.7705	0.3819	0.7705	0.2769	0.3886
S3	0.7562	0.2729	0.1178	0.2729	0.7562	0.1551
S4	0.6975	0.7526	0.1169	0.7526	0.6975	0.6357

Table 2
Cell vectors and angles between them for original and Niggli-reduced cells.

	Cell vectors, Å			Angles, °		
Source data	6.4179	6.5100	6.4610	121.10	88.38	106.47
Transformed data	6.3775	6.4179	6.4610	91.62	119.07	105.12

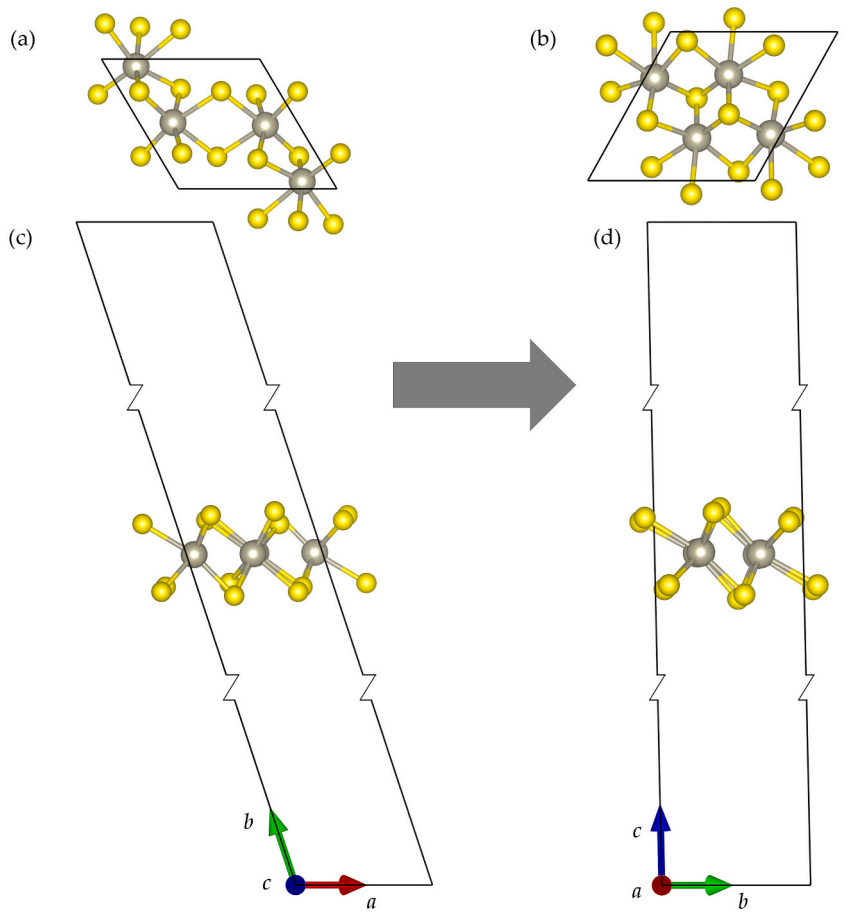

Fig. 2. Initial and Niggli-rebuilt ReS_2 monolayer: top view of ReS_2 monolayer obtained directly from bulk ReS_2 in Niggli form (a); top view of ReS_2 monolayer reached Niggli form (b); side view of ReS_2 monolayer obtained directly from bulk ReS_2 in Niggli form (c); side view of the ReS_2 monolayer reached Niggli form (d). Cells along the axis, perpendicular to the vacuum layer, have additional fractures for a more compact representation.

layered nanomaterial for theoretical and experimental investigations and practical approaches [38–41].

Consider more detailed slab unit cell transformations in the case of ReS_2. First, we obtained a slab from the ReS_2 Niggli-reduced cell by adding a 25 Å vacuum layer in the b-axis direction (which is perpendicular to the layer propagation), so that its lattice vector changed from 6.4179 Å to 28.5019 Å (Fig. 2a–c). The thickness of the vacuum layer was chosen to better demonstrate its influence in band structure analysis. Adjustment of the obtained slab unit cell to Niggli form is accompanied by permutation, a modified direction and strong changes in angles between cell vectors (Fig. 2b). Details of the changes are summarized in Tables 3 and 4. Permutations and changes to cell vectors and Wyckoff positions of atoms result in the source vacuum layer not being saved and decreasing by 1.29971 Å.

In principle, the loss is only 5.2% of the original vacuum layer thickness, but in cases where this original thickness is minimal, it can affect your result. For a consistent approach, we additionally redefined the vacuum layer thickness to the original 25 Å and this final slab unit cell satisfies the Niggli shape. After all transformations, the artificial unit cell of the ReS_2 slab becomes a primitive oblique unit cell belonging to the monoclinic syngony and $P\bar{1}$ layer groups.

The final slab parameters with the recovered vacuum layer are given in Tables 3 and 4, their appearance is shown in Fig. 2 (b, d).

3. Computational details

All calculations were performed within the density functional theory and pseudopotential theory, as implemented in the OpenMX package [42–44], whose source code is freely available under the GNU General Public License version 3 (GPLv3).

The convergence criterion (for the electronic energy) of the self-consistent field calculation was set to 10^{-6} eV/ion for the structure relaxation methods and to 10^{-9} eV for the calculation of all other fixed geometry properties. To achieve convergence, we used the residual minimization method in the direct inversion iterative subspace for charge mixing [45]. The electronic smearing temperature is 300 K.

Before calculating properties, we performed structure relaxation of the ReS_2 bulk and slab. Bulk ReS_2 in Niggli form was relaxed without any constraints for cell vectors and their angles and ionic positions due to the low symmetry of the material until the space group was saved. In the slab case, ionic positions were relaxed without any constraint, while the periodic conditions (cell vectors and their angles of an artificial slab primitive cell) were fixed until the space group was saved. The stopping criterion for a structure relaxation procedure was the achievement value of any component of forces acting on ions or stress tensor equal to or less than 10 meV/Å.

The electronic density was integrated over the first BZ on a Γ-centered regular k-points grid of dimensions $4 \times 5 \times 5$ and $4 \times 4 \times 1$ for the bulk and slab, respectively. The grid for the numerical integration has dimensions $52 \times 46 \times 48$ points in the bulk material case and $49 \times 50 \times 250$ in the slab case, respectively, which is approximately equal to the mean cut-off energy of 210–215 Rydberg in both cases studied.

We used a valence-split basis set with two optimized basis functions for each electron and one additional optimized basis function as a polarization. This is necessary for a more accurate consideration of chemical bonding in the crystal and the correct reproduction of energy band dispersion. 5s, 5p, 5d, and 6s electrons for rhenium, 3s and 3p electrons for sulfur, and 2s and 2p electrons for carbon and oxygen were treated as valence within norm-conserving pseudopotentials.

All calculations were performed within the local density approximation. Exchange and correlation energies were treated within the scheme proposed by Ceperley and Alder and subsequently parametrized by Perdew and Zunger [46,47]. This choice was made due to the possibility of a good description of the structural properties of layered materials with van der Waals interaction between layers, including both classical hexagonal MoS_2 (WS_2) and triclinic ReS_2 [19,48,49]. We checked the ReS_2 bulk and slab and found no spin polarization. This is due to the even number of electrons in all cases studied, which allows us to perform all calculations in a no-spin-polarized approach.

The electronic density of states was calculated using the tetrahedron method over a Γ-centered regular grid of k-points of dimensions $5 \times 6 \times 6$ and $5 \times 5 \times 1$ for bulk and slab, respectively. Population analysis was performed using both the Mulliken and Voronoi approaches. Molecular orbitals were calculated at special high symmetry points of the Brillouin zone, which are relevant extremums of valence and conductance bands.

The atomic (crystal) structure of the bulk and monolayer slab of ReS_2, the difference in electronic density from a superposition of the atomic densities of the constituent atoms, and the molecular orbitals were visualized using the VESTA package.

Table 3
Wyckoff position of rhenium and sulfur atoms for the slab unit cell after straightaway slab fabrication from the bulk, for the slab after casting to Niggli form, and for the slab unit cell cast to Niggli for the recovered vacuum layer.

Unique atom	Wyckoff positions								
	Slab from bulk			Slab in Niggli form			Slab in Niggli form with recovered vacuum layer		
	x	y	z	x	y	z	x	y	z
Re1	0.05640	0.49831	0.80870	0.05978	0.68961	0.49831	0.05978	0.68961	0.49839
Re2	0.51120	0.50059	0.21380	0.51002	0.28679	0.50059	0.51002	0.28679	0.50056
S1	0.24980	0.43637	0.88220	0.37706	0.55417	0.43637	0.37706	0.55417	0.43928
S2	0.77050	0.44976	0.38860	0.87098	0.06116	0.44976	0.87098	0.06116	0.45206
S3	0.27290	0.55769	0.15510	0.15752	0.40259	0.55769	0.15752	0.40259	0.55505
S4	0.75260	0.54447	0.63570	0.66366	0.90877	0.54447	0.66366	0.90877	0.54244

Table 4
Cell vectors and angles between them for the slab unit cell after straightaway slab fabrication from the bulk, for the slab after casting to Niggli form, and for the slab unit cell cast to Niggli for the recovered vacuum layer.

Form of slab	Cell vectors, Å			Angles, °		
Source	6.3775	28.5019	6.4610	91.62	119.07	105.12
Niggli form	6.3775	6.4610	27.1424	88.86	85.39	60.93
Niggli form with a recovered vacuum layer	6.3775	6.4610	28.4421	88.86	85.39	60.93

4. Results and discussion

Analyzing the electronic band structure of ReS_2 is not as straightforward as it may appear, even in the case of bulk form. The introduction delineates the reasons for this complexity. But even if we focus solely on the triclinic case, it does not resolve the primary complication – how to accurately select the Brillouin zone of the triclinic "artificial" slab unit cell for the monolayer. In other words, which specific special high-symmetry points in the first Brillouin zone should we utilize to illustrate the dispersion of electronic bands?

The initial simplistic approach involves utilizing the identical Brillouin zone (BZ) for both the slab and bulk cases. In this approach, both Bravais lattices and Brillouin zones are three-dimensional. Thereby, the coordinates of special high-symmetry points (in scaled units) are recorded, with only the distance between these points in reciprocal space being altered. Thus, ReS_2 (or related compounds), being two-dimensional, is considered three-dimensional, or, more exactly, quasi-three-dimensional. In Fig. 3, we present the electronic band structure of ReS_2 in bulk and monolayer forms, as obtained using the approach described above.

Bulk ReS_2 is a direct band gap semiconductor, with the first electron transition situated at point **X** of the Brillouin zone. The band gap amounts to 1.20 eV, which is slightly lower than our previous findings of 1.26 eV [23], and can be attributed to differences in cell parameters and atomic positions. Overall, our results are in agreement with other calculations and experimental measurements [50–53]. In the case of the ReS_2 slab, it is a (quasi)direct band gap semiconductor with a doubly degenerated valence band maximum located at points that are near the gamma point and belong to the k-path segments **Γ–R** and **Γ–V**. At the gamma point, the valence band is located below 3.3 meV, which is almost eight times lower than the room-temperature energy. It means that this material allows direct transitions at the gamma point even at low temperatures. The transition from bulk to slab is accompanied by an increase in the band gap up to 1.45 eV. Relatively small changes (only 0.25 eV) indicate that quantum confinement in this substance is not as clearly expressed as in close TMDs such as MoS_2 and WS_2. Unlike the difference in hexagonal two-dimensional TMDs, where the extremes of the bands are located at the **K** point, in ReS_2, the extremes are at or near the gamma point. The dispersion of the valence and conductance bands is clearly defined along all segments of a k-path for both the bulk and slab cases of ReS_2. The k-path segment lengths also show noticeable changes in the case of the ReS_2 slab, with the most significant alterations occurring in the **Γ-Z** segment. Also, the dispersion of electronic bands in this segment is linear.

This phenomenon results from describing a ReS_2 monolayer as a quasi-three-dimensional system with one cell vector significantly larger than the other. The limiting case of the slab approach is to equate one of the cell vectors to infinity, which is equivalent to a transition from three dimensions to two. Further increasing this cell vector will cause certain k-path segments to increase while others decrease, leading to unphysical results such as the **Γ-Z** segment being zero at infinite cell vector values.

So, the naive quasi-three-dimensional approach of describing a two-dimensional system as three-dimensional is not accurate exactly. An alternative is to use a two-dimensional Bravais grating and its Brillouin zone. In the context of our investigation, we consider and analyze the oblique, two-dimensional Bravais lattice of the ReS_2 monolayer. Fig. 4 shows a comparison of the electronic band structure of the ReS_2 monolayer treated in both quasi-three-dimensional and two-dimensional cases.

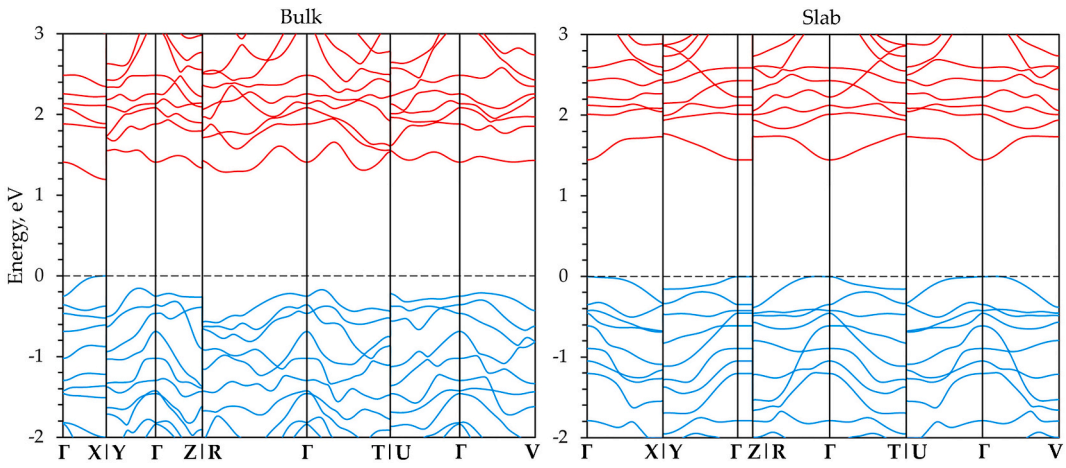

Fig. 3. Electronic band structure of ReS_2. Left panel – bulk shape (three-dimensional); right panel – monolayer (treated as quasi-three-dimensional). Zero is the upper valence band.

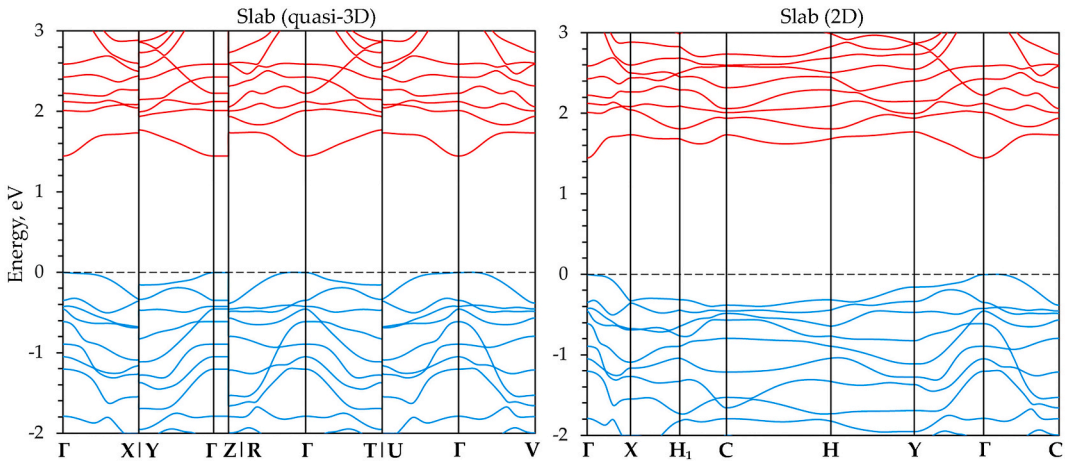

Fig. 4. Electronic band structure of ReS_2 monolayer, which unit cell is treated as quasi-3D (left panel) and as 2D (right panel). Zero is the upper valence band.

The band gap amounts to 1.45 eV in both cases due to the first direct electronic transition located at the gamma point. The lengths of the k-path segments are independent of the largest cell vector, which excludes its influence on the electronic band dispersion representation. Thus, in this approach, vacuum layer thickness is influenced only by the van der Waals interaction, which allows the selection of different vacuum layer thicknesses for the study of two-dimensional materials, ultrathin films, and surfaces and correctly analyzing their band dispersion. Table 5 collects the values of intraband transitions at specific high symmetry points for all cases considered.

The OpenMX code, due to the localized basis set as a linear combination of pseudo-atomic orbitals, allows the calculation of molecular orbitals commonly used and analyzed in molecular quantum chemistry. We calculated the upper two bands from the valence region and the bottom two bands from the conductance region of both bulk and monolayer ReS_2. The isosurface map of these molecular orbitals was visualized using the VESTA package and is shown in Fig. 5. The isovalue was set to equal 0.05 in all cases. Also, in all cases, the view is given in a direction perpendicular to the ReS_2 layer propagation. Despite external differences in an atomic structure, there are very noticeable differences in the shapes and localizations of the molecular orbitals of the crystal in three- and two-dimensional cases. In summary, we can say that quantum confinement leads to the fact that the shapes of molecular orbitals are sharp and clearer, with localization both on atoms and bonds, while in the bulk case, the form of molecular orbitals is more extended and smoothed, with mainly localization on atoms.

The electronic density of states of ReS_2 in the bulk and monolayer cases is shown in Fig. 6. The contribution of the basis set polarization functions is not included due to its small size. In both cases, the valence bands in the energy range shown are formed approximately equally by the contribution of rhenium and sulfur electron states. The near-valence band maximum in the monolayer case is sharper than in the bulk. Conductance bands formed mainly due to the contribution of rhenium ion electron states. Their value is approximately twice larger than the contribution of sulfur ion electron states. This is explained by the decreasing Re–S bond length due to the van der Waals interaction being turned off and, consequently, a little bit of monolayer compression. Besides the sharper shape, the DOS increases due to the contribution of Re electronic states. Turning off the van der Waals interaction also results in a more defined, atomic-like, non-smoothed shape of the DOS curve of the conductance bands, which is in good agreement with the calculated band structure. Analysis of the orbital-projected DOS shows that the valence bands form p- and d-states, with the contribution of s-states expectedly small. At the same time, conductance bands form p- and, to a greater extent, d-states. In addition, Re-e_g and Re-t_{2g} states contributions were calculated. In the valence band region, up to 0.4 eV, the deep contribution of both states is nearly equal and increases slightly with depth for t_{2g} states. In the conductance band region, the contributions of the t_{2g}-states are expectedly larger. In

Table 5
Intraband transition values at special high-symmetry points for ReS_2 bulk, monolayer as a quasi-3D structure, and monolayer as a 2D structure.

Special point	Bulk	Slab (quasi-3D)	Special point	Slab (2D)
	Transition, eV			Transition, eV
Γ	1.661	1.449	**Γ**	1.449
X	1.197	2.063	**X**	2.063
Y	2.057	1.927	**H_1**	2.001
Z	1.602	1.449	**C**	2.115
R	1.986	2.115	**H**	2.001
T	1.969	1.927	**Y**	1.927
U	1.776	2.063		
V	1.861	2.115		

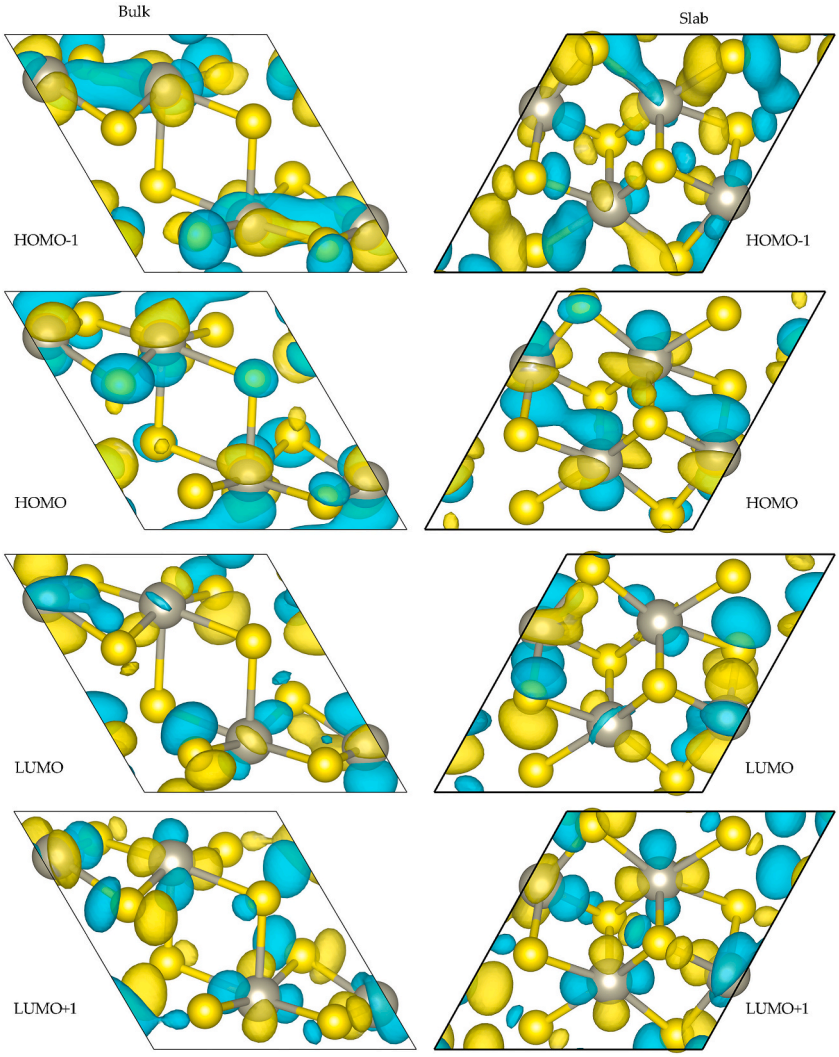

Fig. 5. Isosurface map of the molecular orbitals of the bulk of ReS_2 (left panel) and the monolayer of ReS_2 (right panel). The isovalue is set to 0.05.

general, a decrease in the dimensionality of ReS_2 is accompanied by smaller manifestations of the distribution of electronic density of state changes due to quantum confinement than for other TMDs and other popular materials with a more high-symmetrical structure [54–56], which is related to the low-symmetry nature of the crystal structure of this material.

Analyzing the electron difference density taken from a superposition of atomic densities of a constituent atom (Fig. 7) shows that their shapes and volumes in the two-dimensional case are more continuous and tighter filling interatomic space than bulk case. At the same time, partial reorientation of electronic difference densities along the c-axis is observed due to turning off both Coulomb and van der Waals interactions in a two-dimensional case. Nevertheless, independent of dimensionality, the electron difference distribution, in general, is saved, which also says about the weakness of quantum confinement in this material.

In addition, we performed a population analysis of ReS_2 in both bulk and slab forms. In quantum chemistry, there are many methods for analyzing effective charges in finite systems. For periodical systems, not all of these methods are implemented, but some methods are available. Particularly within the OpenMX code, due to the localized basis set available for electron population analysis in the Mulliken and Voronoi approaches, which gives some effective charges (Table 6).

Of course, examination of Mulliken population analysis results, popular and justified for finite systems, must be more thoughtful in the case of periodical systems, even two-dimensional. Nevertheless, this approach is useful in our case for the qualitative analysis of reducing dimensionality. The transition from bulk to two-dimensional form is accompanied by is an increase in 1.5 times the effective charge on rhenium ions and 1.1–2.5 times the effective charge on sulfur ions, depending on their positions. This is explained by screening rhenium ions for sulfur ions, which, after turning off any interactions between layers, redistribute electron density between themselves, as confirmed by electron difference density maps (see Fig. 7). Increasing effective charge values shows that reducing dimensionality promotes the localization of electron density on atoms. Unfortunately, Mulliken population analysis does not show electron density changes in crystal space around each atom. This information may be obtained from the Voronoi charge analysis. In this

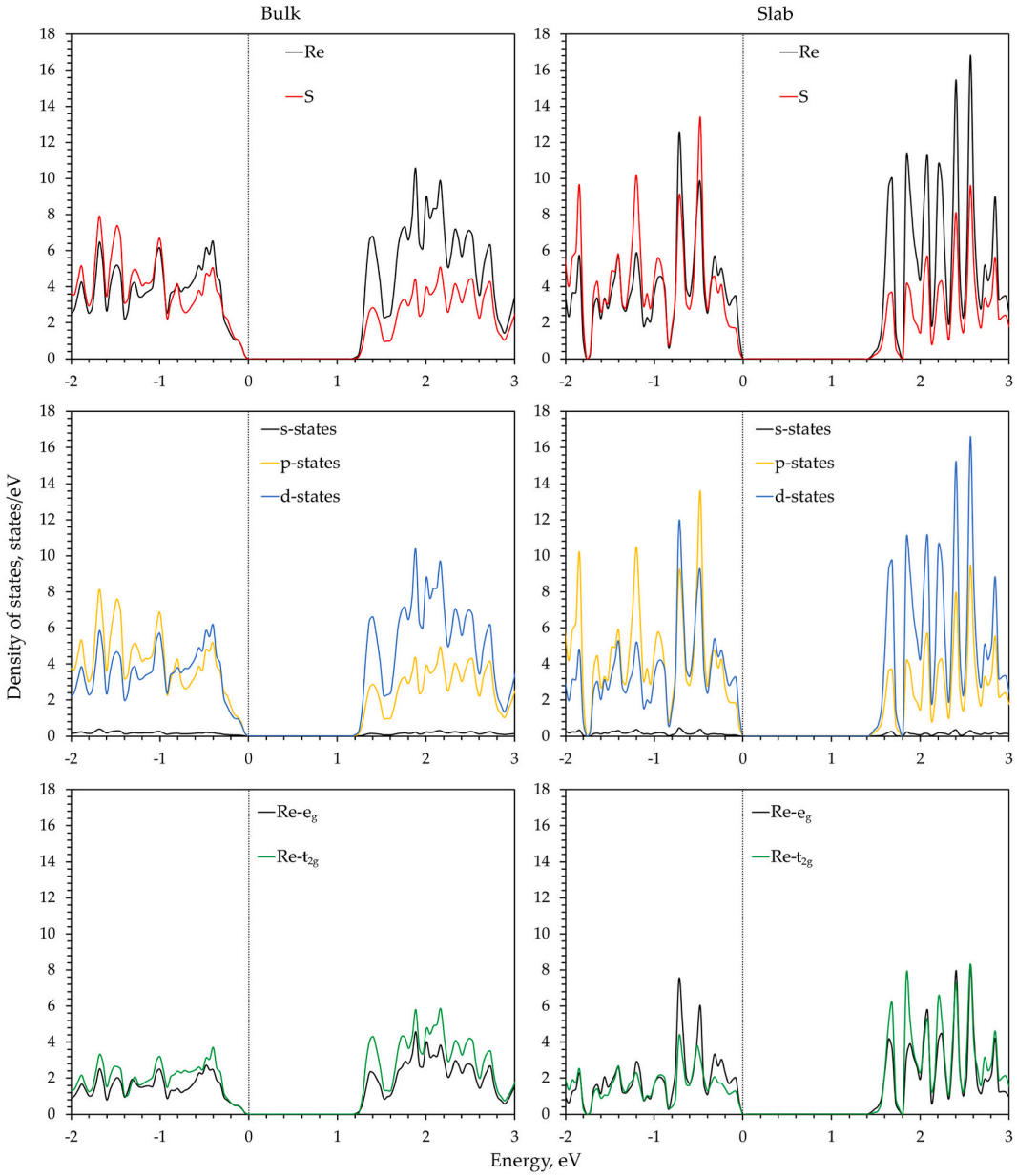

Fig. 6. The electronic density of states (DOS) of ReS_2 in bulk (left panels) and monolayer (right panels) forms. Top row – species-projected DOS; middle row – orbital-projected DOS; bottom row – Re-5d electronic DOS, distributed by symmetry. Zero is the upper valence band. The contribution of the polarization functions is not included.

case, effective charge (Voronoi charge) is calculated by integrating electron and spin densities in a Voronoi polyhedron. It should be noted that the Voronoi polyhedron is determined by only the structure, and their volumes are not saved for transition bulk to slab form, as in our case. Nevertheless, it doesn't affect changes in effective charges, which are less than 1–2% for all ions. Combining either approach, we can say that the quantum confinement effect is weak in ReS_2 due to the "insensitivity" of the electronic subsystem in the material to structural rebuilding within reducing dimensionality owing to the low symmetry structure and weak interaction of localized electrons.

5. Conclusion

The structural and electronic properties of rhenium disulfide in different forms – three-dimensional bulk and two-dimensional monolayer – were studied within density functional theory and pseudopotentials. A new routine for standardizing bulk and "artificial" slab unit cells of ReS_2 descriptions based on their casting to Niggli form was proposed. A detailed description of these

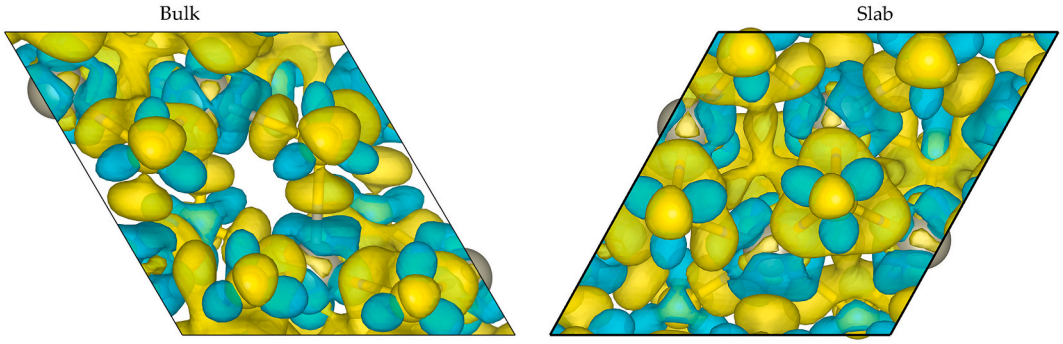

Fig. 7. Top view on isosurface map of difference electron density, which is taken from a superposition of atomic densities of a constituent atom for the ReS_2 bulk (left panel) and the ReS_2 monolayer (right panel). The isovalue is set to 0.05.

Table 6
Effective charges by Mulliken and Voronoi population analysis for the bulk and slab of ReS_2.

Unique atom	Populations by			
	Mulliken		Voronoi	
	Bulk	Slab	Bulk	Slab
Re1	+0.08	+0.12	+0.99	+1.00
Re2	+0.07	+0.11	+1.00	+1.01
S1	−0.02	−0.04	−0.45	−0.45
S2	−0.04	−0.06	−0.51	−0.51
S3	−0.02	−0.05	−0.47	−0.48
S4	−0.08	−0.09	−0.56	−0.56

transformations is provided for both bulk and "artificial" slab unit cells, which were obtained reconstruction of bulk unit cells. The vacuum layer thickness influence on choosing specified special high-symmetry points was discussed. It was shown that an "artificial" slab unit cell is three-dimensional and leads to a quasi-three-dimensional description of two-dimensional structures and thin films based on ReS_2 as well as related low-symmetry compounds. Such incompleteness of the classical slab approach can be improved by considering an "artificial" unit cell as two-dimensional that excludes the influence of a vacuum layer (with a sufficient thickness of it) on reciprocal vector lengths, and simplifies the building, and analyzes band dispersion along specified special high-symmetry points in the first two-dimensional Brillouin zone. Electron band dispersion in both the classical quasi-three-dimensional Brillouin zone and the proposed two-dimensional approach was compared. It was established that the proposed two-dimensional approach is preferable for low-symmetry crystals such as ReS_2.

It was shown that the bulk ReS_2 is a direct gap semiconductor with a band gap of 1.20 eV. The direct transition lies in the X point of the first BZ, which agrees with experimental data and published results of other calculations. The transition from bulk to monolayer was accompanied by an increasing band gap up to 1.45 eV, with a direct transition towards the BZ center. The transition situated directly at the Γ-point lies 3.3 meV below the first direct transition located near this point. Thus, a monolayer of ReS_2 is a direct gap semiconductor in a wide range of temperatures, excluding only a narrow range at low temperatures, where it acts as a quasi-direct gap semiconductor. In both cases, valence bands are formed approximately equally by the contribution of rhenium and sulfur ions to electron states, while conductance bands principally form the contribution of rhenium ions to electron states, which is twice larger than the contribution of sulfur ions to electron states. These patterns are saved for both bulk and monolayer forms of the studied material. In the valence bands, both t_{2g}- and e_g-states contribute nearly equally, and the t_{2g}-states show a slight increase with energy depth. In the conductance bands, the t_{2g}-states have larger contributions.

It has been demonstrated that in the bulk case, molecular orbitals take a more extended and smooth form, with localization primarily on atoms. In contrast, in cases of dimension reduction, the orbital shapes become sharper and clearer, with a localized presence on both atoms and bonds. It is correlated with the results of the electron difference density, obtained from a superposition of the atomic densities of a constituent atom. It shows that shapes and volumes in the bulk case are less continuous and have less filling of interatomic space with partial reorientation of the electronic difference densities along the c-axis than in the two-dimensional case.

Finally, we used two different approximations of population analysis — Mulliken and Voronoi — to figure out the effective charges of rhenium and sulfur ions. The Mulliken approach revealed that dimension reduction leads to the effective charges increasing by 1.5 times for rhenium ions and 1.1 to 2.5 times for sulfur ions, depending on their positions. On the other hand, the Voronoi approximation showed almost no change in effective charges, indicating that the change in electronic density principally occurred only near the ions and almost not changed in the volume constrained by the Voronoi polyhedron.

The summary of the presented data allows the quantified estimation and explanation of the severity of the weak quantum confinement effect in rhenium disulfide that was experimentally observed. The results may be useful for creating atomic models of

ReS_2-based structures or other low-symmetrical compounds for consequent theoretical description and modeling of a wide range of properties.

Funding

The authors would like to extend their sincere appreciation to the Researchers Supporting Project Number (RSP2024R301), King Saud University, Riyadh, Saudi Arabia. The work was performed with supporting of State Program of Scientific Research "Material Science, New materials and Technology" in frame of assignment 2.14.3, Republic of Belarus.

Data Availability Statement

The article provides all the information needed to perform similar calculations. The data sets generated and/or analyzed during the current study are available from the corresponding author upon reasonable request.

Compliance with ethical standards

Not applicable.

CRediT authorship contribution statement

Aleksey Baglov: Writing – review & editing, Writing – original draft, Visualization, Validation, Software, Methodology, Investigation, Funding acquisition, Data curation, Conceptualization. **Liudmila Khoroshko:** Writing – review & editing, Writing – original draft, Visualization, Validation, Supervision, Software, Project administration, Methodology, Investigation, Formal analysis, Data curation, Conceptualization. **Anastasiya Zhoidzik:** Software, Resources, Investigation. **Mengge Dong:** Writing – review & editing, Validation. **Qunhong Weng:** Writing – review & editing. **Mohsin Kazi:** Writing – review & editing, Data curation. **Mayeen Uddin Khandaker:** Writing – review & editing, Funding acquisition. **Mohammad Aminul Islam:** Validation, Resources. **Zaira Zaman Chowdhury:** Validation, Project administration. **M.I. Sayyed:** Validation, Investigation. **Sergei Trukhanov:** Writing – review & editing. **Daria Tishkevich:** Writing – original draft, Resources, Funding acquisition. **Alex Trukhanov:** Supervision, Conceptualization.

Declaration of competing interest

The authors declare that they have no known competing financial interests or personal relationships that could have appeared to influence the work reported in this paper.

The authors declare the following financial interests/personal relationships which may be considered as potential competing interests.

Acknowledgments

The authors would like to extend their sincere appreciation to the Researchers Supporting Project Number (RSP2024R301), King Saud University, Riyadh, Saudi Arabia. Authors are very grateful to Dzianis A. Asinenka for his assistance in organizing and carrying out the procedure of calculations.

References

[1] M.A. Lukowski, A.S. Daniel, F. Meng, A. Forticaux, L. Li, S. Jin, Enhanced hydrogen evolution Catalysis from chemically Exfoliated Metallic MoS_2 nanosheets, J. Am. Chem. Soc. 135 (28) (2013) 10274–10277, https://doi.org/10.1021/ja404523s.

[2] D. Voiry, M. Salehi, R. Silva, T. Fujita, M. Chen, T. Asefa, V.B. Shenoy, G. Eda, M. Chhowalla, Conducting MoS_2 nanosheets as catalysts for hydrogen evolution reaction, Nano Lett. 13 (12) (2013) 6222–6227, https://doi.org/10.1021/nl403661s.

[3] K. Chang, W. Chen, L-Cysteine-Assisted Synthesis of layered MoS2/graphene composites with Excellent electrochemical Performances for lithium ion batteries, ACS Nano 5 (6) (2011) 4720–4728, https://doi.org/10.1021/nn200659w.

[4] D.J. Late, R.V. Kanawade, P.K. Kannan, C.S. Rout, Atomically thin WS_2 nanosheets based gas sensor, Sens. Lett. 14 (12) (2016) 1249–1254, https://doi.org/10.1166/sl.2016.3764.

[5] F. Wu, H. Tian, Y. Shen, Z. Hou, J. Ren, G. Gou, Y. Sun, Y. Yang, T.-L. Ren, Vertical MoS_2 transistors with sub-1-nm gate lengths, Nature 603 (2022) 259–264, https://doi.org/10.1038/s41586-021-04323-3.

[6] M. Shahrokhi, P. Raybaud, T. Le Bahers, On the understanding of the optoelectronic properties of S-doped MoO_3 and O-doped MoS_2 bulk systems: a DFT perspective, J. Mater. Chem. C 8 (2020) 9064–9074, https://doi.org/10.1039/D0TC02066D.

[7] M. Shahrokhi, T. Le Bahers, P. Raybaud, Tailoring the optoelectronic properties and dielectric profiles of few-layer S-doped MoO_3 and O-doped MoS_2 nanosheets: a first-principles study, Phys. Chem. Chem. Phys. 24 (2022) 25440–25451, https://doi.org/10.1039/D2CP03410G.

[8] M. Shahrokhi, P. Raybaud, T. Le Bahers, 2D $MoO_{3-x}S_x/MoS_2$ van der Waals Assembly: a tunable Heterojunction with attractive properties for Photocatalysis, ACS Appl. Mater. Interfaces 13 (30) (2021) 36465–36474, https://doi.org/10.1021/acsami.1c08200.

[9] X. Xu, H. Zhao, R. Wang, Z. Zhang, X. Dong, J. Pan, J. Hu, H. Zeng, Identification of few-layer ReS_2 as photo-Electro integrated catalyst for hydrogen evolution, Nano Energy 48 (2018) 337–344, https://doi.org/10.1016/j.nanoen.2018.03.078.

[10] Y. Zhou, E. Song, J. Zhou, J. Lin, R. Ma, Y. Wang, W. Qiu, R. Shen, K. Suenaga, Q. Liu, J. Wang, Z. Liu, J. Liu, Auto-optimizing hydrogen evolution Catalytic Activity of ReS_2 through Intrinsic charge Engineering, ACS Nano 12 (5) (2018) 4486–4493, https://doi.org/10.1021/acsnano.8b00693.

[11] J. Gao, L. Li, J. Tan, H. Sun, B. Li, J.C. Idrobo, C.V. Singh, T.-M. Lu, N. Koratkar, Vertically oriented arrays of ReS_2 nanosheets for electrochemical energy Storage and Electrocatalysis, Nano Lett. 16 (6) (2016) 3780–3787, https://doi.org/10.1021/acs.nanolett.6b01180.

[12] F. Liu, S. Zheng, X. He, A. Chaturvedi, J. He, W.L. Chow, T.R. Mion, X. Wang, J. Zhou, Q. Fu, H.J. Fan, B.K. Tay, L. Song, R.-H. He, C. Kloc, P.M. Ajayan, Z. Liu, Highly sensitive detection of polarized light using anisotropic 2D ReS_2, Adv. Funct. Mater. 26 (2016) 1169–1177, https://doi.org/10.1002/adfm.201504546.

[13] E. Liu, M. Long, J. Zeng, W. Luo, Y. Wang, Y. Pan, W. Zhou, B. Wang, W. Hu, Z. Ni, Y. You, X. Zhang, S. Qin, Y. Shi, K. Watanabe, T. Taniguchi, H. Yuan, H. Y. Hwang, Y. Cui, F. Miao, D. Xing, High Responsivity phototransistors based on few-layer ReS2 for weak signal detection, Adv. Funct. Mater. 26 (2016) 1938–1944, https://doi.org/10.1002/adfm.201504408.

[14] C.M. Corbet, C. McClellan, A. Rai, S.S. Sonde, E. Tutuc, S.K. Banerjee, Field effect transistors with current Saturation and Voltage Gain in ultrathin ReS2, ACS Nano 9 (1) (2015) 363–370, https://doi.org/10.1021/nn505354a.

[15] M.Z. Rahman, K. Davey, S.-Z. Qiao, Advent of 2D rhenium disulfide (ReS_2): Fundamentals to applications, Adv. Funct. Mater. 27 (2017) 1606129, https://doi.org/10.1002/adfm.201606129.

[16] H.H. Murray, S.P. Kelty, R.R. Chianelli, C.S. Day, Structure of rhenium disulfide, Inorg. Chem. 33 (19) (1994) 4418¬–4420, https://doi.org/10.1021/ic00097a037.

[17] R. Coehoorn, C. Haas, J. Dijkstra, C.J.F. Flipse, de R.A. Groot, A. Wold, Electronic structure of MoSe2, MoS2, and WSe2. I. Band-structure calculations and photoelectron spectroscopy, Phys. Rev. B 35 (1987) 6195, https://doi.org/10.1103/PhysRevB.35.6195.

[18] W.J. Schutte, J.L. De Boer, F. Jellinek, Crystal structures of tungsten disulfide and diselenide, J. Solid State Chem. 70 (2) (1987) 207–209, https://doi.org/10.1016/0022-4596(87)90057-0.

[19] C.H. Ho, Y.S. Huang, J.L. Chen, T.E. Dann, K.K. Tiong, Electronic structure of ReS_2 and $ReSe_2$ from first-principles calculations, photoelectron spectroscopy, and electrolyte electroreflectance, Phys. Rev. B 60 (1999) 15766, https://doi.org/10.1103/PhysRevB.60.15766.

[20] B.K. Choi, S. Ulstrup, S.M. Gunasekera, J. Kim, S.Y. Lim, L. Moreschini, J.S. Oh, S.-H. Chun, C. Jozwiak, A. Bostwick, E. Rotenberg, H. Cheong, I.-W. Lyo, M. Mucha-Kruczynski, Y.J. Chang, Visualizing orbital content of electronic bands in anisotropic 2D semiconducting $ReSe_2$, ACS Nano 14 (7) (2020) 7880–7891, https://doi.org/10.1021/acsnano.0c01054.

[21] D. Biswas, A.M. Ganose, R. Yano, J.M. Riley, L. Bawden, O.J. Clark, J. Feng, L. Collins-Mcintyre, M.T. Sajjad, W. Meevasana, T.K. Kim, M. Hoesch, J.E. Rault, T. Sasagawa, D.O. Scanlon, P.D.C. King, Narrow-band anisotropic electronic structure of ReS_2, Phys. Rev. B 96 (2017) 085205, https://doi.org/10.1103/PhysRevB.96.085205.

[22] S.M. Gunasekera, D. Wolverson, L.S. Hart, M. Mucha-Kruczynski, Electronic band structure of rhenium dichalcogenides, J. Electron. Mater. 47 (2018) 4314–4320, https://doi.org/10.1007/s11664-018-6239-0.

[23] A.V. Baglov, L.S. Khoroshko, Crystal structure and electronic properties of rhenium disulfide, J. Appl. Spectrosc. 89 (2022) 860–864, https://doi.org/10.1007/s10812-022-01438-x.

[24] H.J. Lamfers, A. Meetsma, G.A. Wiegers, J.L. de Broer, The crystal structure of some rhenium and Technetium dichalcogenides, J. Alloy. Compd. 241 (1–2) (1996) 34–39, https://doi.org/10.1016/0925-8388(96)02313-4.

[25] C. Kittel, Introduction to Solid State Physics, eighth ed., Wiley, New York. USA, 2005.

[26] E. Parthé, Elements of Inorganic Structural Chemistry: a Course on Selected Topics; K. Sutter Parthé: Petit-Lancy, 1990. Switzerland.

[27] I. Křivý, B. Gruber, A unified algorithm for determining the reduced (Niggli) cell, Acta Cryst A32 (1976) 297–298, https://doi.org/10.1107/S0567739476000636.

[28] A. Santoro, A.D. Mighell, Determination of reduced cells, Acta Cryst A26 (1970) 124–127, https://doi.org/10.1107/S0567739470000177.

[29] B. Gruber, The relationship between reduced cells in a general Bravais lattice, Acta Cryst A29 (1973) 433–440, https://doi.org/10.1107/S0567739473001063.

[30] G. Eisenstein, Tabelle der reducirten positiven ternären quadratischen Formen, nebst den Resultaten neuer Forschungen über diese Formen, in besonderer Rücksicht auf ihre tabellarische Berechnung, J. Math. 41 (1851) 141–190, https://doi.org/10.1515/crll.1851.41.141.

[31] P. Niggli, Handbuch der Experimentalphysik, vol. 7, Leipzig: Akademische Verlagsgesellschaft, Germany, 1928. Part 1.

[32] L.V. Azaroff, M.J. Buerger, The Powder Method in X-Ray Crystallography, McGraw-Hill Book Co. Inc., New York, USA, 1958, 1958.

[33] L.M. Gelato, E. Parthé, Structure TIDY – a Computer program to standardize crystal structure data, J. Appl. Cryst. 20 (1987) 139–143, https://doi.org/10.1107/S0021889887086965.

[34] K. Momma, F. Izumi, VESTA 3 for three-dimensional visualization of crystal, volumetric and morphology data, J. Appl. Crystallogr. 44 (2011) 1272–1276, https://doi.org/10.1107/S0021889811038970.

[35] Shiraishi, K. A new slab model approach for electronic structure calculation of polar semiconductor surface. J. Phys. Soc. Japan, 1190, 59(10), 3455–3458. https://doi.org/10.1143/jpsj.59.3455.

[36] O. Lisovski, S. Piskunov, D. Bocharov, S. Kenmoe, 2D slab models of Nanotubes based on Tetragonal TiO_2 structures: Validation over a Diameter range, Nanomaterials 11 (2021) 1925, https://doi.org/10.3390/nano11081925.

[37] J. Zhang, Y. Zhao, X. Guo, Chung-Li Dong, Ru-Shi Liu, Chih-Pin Han, Yadong Li, Yury Gogotsi, Guoxiu Wang, Single platinum atoms immobilized on an MXene as an efficient catalyst for the hydrogen evolution reaction, Nat. Catal. 1 (2018) 985–992, https://doi.org/10.1038/s41929-018-0195-1.

[38] A. Devi, N. Dhiman, N. Kumar, W. Alfalasi, A. Kumar, P.K. Ahluwalia, A. Singh, N. Tit, Ferromagnetism in Defected TMD (MoX_2, X = S, Se) monolayer and its Sustainability under O_2, O_3, and H_2O gas Exposure: DFT study, Nanomaterials 13 (2023) 1642, https://doi.org/10.3390/nano13101642.

[39] M.S. Ramzan, C. Cocchi, Strained monolayer $MoTe_2$ as a Photon Absorber in the Telecom range, Nanomaterials 13 (2023) 2740, https://doi.org/10.3390/nano13202740.

[40] J.S. Lemos, E. Blundo, A. Polimeni, M.A. Pimenta, A. Righi, Exciton–phonon interactions in Strained Domes of monolayer MoS_2 studied by Resonance Raman spectroscopy, Nanomaterials 13 (2023) 2722, https://doi.org/10.3390/nano13192722.

[41] W. Ali, Y. Liu, M. Huang, Y. Xie, Z. Li, Temperature-Dependent Phonon Scattering and photoluminescence in vertical MoS_2/WSe_2 Heterostructures, Nanomaterials 13 (2023) 2349, https://doi.org/10.3390/nano13162349.

[42] T. Ozaki, Variationally optimized atomic orbitals for Large-Scale electronic structures, Phys. Rev. B 67 (15) (2003) 155108, https://doi.org/10.1103/PhysRevB.67.155108.

[43] T. Ozaki, H. Kino, Numerical atomic basis orbitals from H to Kr, Phys. Rev. B 69 (19) (2004) 195113, https://doi.org/10.1103/PhysRevB.69.195113.

[44] T. Ozaki, H. Kino, Efficient projector Expansion for the ab initio LCAO method, Phys. Rev. B 72 (4) (2005) 045121, https://doi.org/10.1103/PhysRevB.72.045121.

[45] G. Kresse, J. Furthmüller, Efficient iterative schemes for ab initio total-energy calculations using a plane-Wave basis set, Phys. Rev. B 54 (16) (1996) 11169, https://doi.org/10.1103/PhysRevB.54.11169.

[46] D.M. Ceperley, B.J. Alder, Ground state of the electron gas by a Stochastic method, Phys. Rev. Lett. 45 (1980) 566, https://doi.org/10.1103/PhysRevLett.45.566.

[47] J.P. Perdew, A. Zunger, Self-interaction correction to density-functional approximations for many-electron systems, Phys. Rev. B 23 (10) (1981) 5048, https://doi.org/10.1103/PhysRevB.23.5048.

[48] S.S. Coutinho, M.S. Tavares, C.A. Barboza, N.F. Frazão, E. Moreira, D.L. Azevedo, 3R and 2H Polytypes of MoS_2: DFT and DFPT calculations of structural, optoelectronic, Vibrational and Thermodynamic properties, J. of Phys. and Chem. of Solids 111 (2017) 25–33, https://doi.org/10.1016/j.jpcs.2017.07.010.

[49] L. Feng, Z. Wang, Z. Liu, First-principles calculations on Mechanical and Elastic properties of 2H- and 3R-WS_2 under Pressure, Solid State Commun. 187 (2014) 43–47, https://doi.org/10.1088/1742-6596/1634/1/012145.

[50] J.R. Gadde, A. Karmakar, T.K. Maji, S. Mukherjee, R. Alexander, A.M.R. Sharma, S. Das, A. Mandal, K. Dasgupta, A. Naik, K. Majumdar, R. Hawaldar, K. V. Adarsh, S.K. Ray, D. Karmakar, Two-dimensional ReS_2: Solution to the unresolved queries on its structure and inter-layer coupling leading to potential optical applications, Phys. Rev. Materials 5 (2021) 054006, https://doi.org/10.1103/PhysRevMaterials.5.054006.

[51] L.S. Hart, J.L. Webb, S. Dale, S.J. Bending, M. Mucha-Kruczynski, D. Wolverson, C. Chen, J. Avila, M.C. Asensio, Electronic bandstructure and van der Waals coupling of $ReSe_2$ revealed by high-resolution angle-resolved photoemission spectroscopy, Sci. Rep. 7 (2017) 5145, https://doi.org/10.1038/s41598-017-05361-6.
[52] N. Wang, Y. Li, L. Wang, X. Yu, Photocatalytic applications of ReS_2-based Heterostructures, Molecules 28 (2023) 2627, https://doi.org/10.3390/molecules28062627.
[53] K.P. Dhakal, E. Lee, T.V. Anh, G. Ghimire, W. Choi, Y.-M. Kim, D.L. Duong, J. Kim, Investigation of exciton states of ReS_2 by temperature- and polarization-dependent photoluminescence and oxygen plasma treatment, Appl. Surf. Sci. 30 (2023) 158093, https://doi.org/10.1016/j.apsusc.2023.158093.
[54] M. Shahrokhi, C. Leonard, Tuning the band gap and optical spectra of silicon-doped graphene: many-body effects and excitonic states, J. Alloys Compd. 693 (2017) 1185–1196, https://doi.org/10.1016/j.jallcom.2016.10.101.
[55] M. Shahrokhi, C. Leonard, Quasi-particle energies and optical excitations of wurtzite BeO and its nanosheet, J. Alloys Compd. 682 (2016) 254–262, https://doi.org/10.1016/j.jallcom.2016.04.288.
[56] M. Shahrokhi, Quasi-particle energies and optical excitations of ZnS monolayer honeycomb structure, Appl. Surf. Sci. 390 (2016) 377–384, https://doi.org/10.1016/j.apsusc.2016.08.055.